Environment International 146 (2021) 106279

Contents lists available at ScienceDirect

Environment International

journal homepage: www.elsevier.com/locate/envint

A comprehensive study on ozone pollution in a megacity in North China Plain during summertime: Observations, source attributions and ozone sensitivity

Jian Sun [a,b], Zhenxing Shen [a,b,*], Ruonan Wang [b], Guohui Li [b], Yue Zhang [a], Bin Zhang [a], Kun He [a], Zhuoyue Tang [a], Hongmei Xu [a], Linli Qu [c], Steven Sai Hang Ho [d], Suixin Liu [b], Junji Cao [b]

[a] Department of Environmental Science and Engineering, Xi'an Jiaotong University, Xi'an 710049, China
[b] Key Lab of Aerosol Chemistry & Physics, Institute of Earth Environment, Chinese Academy of Sciences, Xi'an 710049, China
[c] Hong Kong Premium Services and Research Laboratory, Kowloon, Hong Kong Special Administrative Region
[d] Divison of Atmospheric Sciences, Desert Research Institute, Reno NV89512, United States

ARTICLE INFO

Handling Editor: Xavier Querol

Keywords:
VOCs
Tropospheric ozone
NO_x
WRF-CHEM
Pollution control

ABSTRACT

Tropospheric ozone (O_3) pollution has been becoming prominent in North China Plain (NCP) in China since last decade. In order to clarify the source contribution and formation mechanism of O_3, the critical precursors of volatile organic compounds (VOCs) were measured with both on-line and off-line methods in Luoyang City in summer of 2019. The concentrations of nitrogen oxides (NO_x, sum of NO and NO_2) and O_3 were simultaneously monitored. Fifty-seven VOCs measured in U.S. Photochemical Assessment Monitoring Station (PAMS) showed daily concentrations in a range of 14.5 ± 5.33 to 29.2 ± 11.2 ppbv in Luoyang, which were comparable with those in other Chinese megacities. The mass compositions of VOCs were determined, with comparatively low proportions of alkanes (<50%) but high fractions of photoreactive alkenes and alkyne. Source apportionment of VOCs was conducted by Hybrid Environmental Receptor Model (HERM). The results indicated that industrial (38.5%) and traffic (32.0%) were the two dominated pollution sources of VOCs in the urban, while the biogenic and residential sources had contributions of 15.8% and 13.8%, respectively. To further measure the O_3 formation sensitivity and its source attribution, the WRF-CHEM model was adopted in this study. The variation of O_3 between the observation and the stimulation using the local emission inventory showed an index of agreement (IOA) of 0.85. The simulation conducted by WRF-CHEM indicated an average of 43.5% of the O_3 was associated with the regional transportation, revealing the importance of inter-regional prevention and control policy. Traffic and biogenic emissions were the two major pollution sources to an O_3 episode occurred from July 21 to July 27, 2019 (when O_3 concentration over 150 μg m^{-3}) in Luoyang, with average contributions of 22.9% and 18.3%, respectively. The O_3 isopleths proved that its formation in the atmosphere of Luoyang was in transitional regime and collectively controlled by both VOCs and NO_x. This was different from the observations in main cities of NCP before implantations of strict emission controls. The isopleths additionally designated that the O_3 formation regime would move forward or shift to NO_x regime after a reduction of over 45% during the episode. Similar patterns were also reported in other Chinese megacities such as Beijing and Shanghai, due to the tightening of the NO_x control policies. Our results do support that the simultaneous controls of NO_x and VOCs were effective in reductions of tropospheric O_3 in Luoyang. Meanwhile, joint regional control policies on the emissions of NO_x and VOCs can potentially overwhelm the current O_3 pollutions in China.

1. Introduction

North China Plain (NCP), as one of the well-developed region and heavy industry centers in China, has been suffering severe ozone (O_3) pollutions since last decade (Lyu et al., 2019; Wang et al., 2017a). High tropospheric O_3 concentrations were demonstrated serious adverse

* Corresponding author at: Department of Environmental Science and Engineering, Xi'an Jiaotong University, Xi'an 710049, China.
E-mail address: zxshen@mail.xjtu.edu.cn (Z. Shen).

https://doi.org/10.1016/j.envint.2020.106279
Received 27 June 2020; Received in revised form 4 November 2020; Accepted 9 November 2020
Available online 1 December 2020

impacts on human health, global climate and atmosphere (Shao et al., 2016; Shen et al., 2014). It is well known that volatile organic compounds (VOCs) and nitrogen oxides (NO_x) are the two key precursors to the tropospheric O_3 formation with complex chemical mechanism (Pollack et al., 2012). The VOCs concentrations varied with emission intensities of pollution sources and meteorological conditions, while the latter factor greatly influences chemical transformation and further impacts the O_3 production (Carter, 2009). Moreover, the ratio of VOCs to NO_x in atmospheric would govern the photochemical processes which play even more crucial role on the O_3 formations (Luecken et al., 2018; Tan et al., 2018). Therefore, it is important to conduct localized source apportionment and determine the O_3 sensitivity to VOCs and NO_x. These could assist to establish effective control strategies.

Numerous studies have been conducted on the observations of ambient VOCs. Offline sampling method was mostly adopted in determination of spatial distributions of VOCs (Ho et al., 2018; Yamada, 2013) due to its portability and accessibility. However, the collection efficiencies might be impacted by the multiple parameters (Ho et al., 2017, 2018). Online VOCs sampling technology is becoming popular (Cui et al., 2016). However, the extremely high costs (i.e., instrumentation, installation and maintenance) limit its applications on the extensive monitoring campaigns. Many previous studies were troubled with the selection of a proper sampling method, thereupon left certain uncertainties and limitations for subsequent chemical analysis.

Receptor models are frequently applied in VOCs source apportionments (Liu et al., 2008b). Even though the massive usages, positive matrix factorization (PMF) and chemical mass balance (CMB) both showed demerits. PMF needs large data sets while CMB requires precise localized VOCs profiles (Hopke, 2016). A new model combining PMF and CMB, namely Hybrid Environmental Receptor Model (HERM), has been developed and demonstrated its superiority in particulate matter (PM) apportionments (Chen and Cao, 2018). Currently, the HERM is rarely used in source apportionment with VOCs data sets.

Weather Research and Forecasting Model with Chemistry (WRF-CHEM) was selected in this study to conduct O_3 source attribution and sensitivity tests. The WRF-CHEM model could resolve meteorology and physical/chemical processes on the pollutant at the same time (Arghavani et al., 2019; Ryu et al., 2019; Su et al., 2017). Furthermore, with the assist of localized emission inventory and vast cases, the WRF-CHEM generally performs well in simulating meteorological parameters and O_3 pollutions against observations in NCP (Guo et al., 2016; Su et al., 2017; Wang et al., 2016; Wu et al., 2018b; Zhang et al., 2017). Localized inventory and observation data in Luoyang were input into the WRF-CHEM model for obtaining a better inversion result. This assists to interpret O_3 episodes and conduct sensitivity studies in Luoyang.

Luoyang, a typical industrial city located in Henan province of China, is suffering severe O_3 pollution. The annual 90th centile maximum 8-h concentration of O_3 ranked top 20 among 364 cities in China since 2016 (Li et al., 2018b). As the city of the second highest gross domestic production (GDP) in Henan, Luoyang has large numbers of petrochemical and furniture manufacturers which are known large producers to ambient VOCs (LBS, 2018). In this study, a comprehensive VOC sampling campaign was conducted in urban and rural sites in Luoyang in summer of 2019. A total of 232 offline VOC samples were collected, and additionally with an intensive 30-day continuous online monitoring of VOCs, NO_x and O_3 in an urban city-center. HERM was firstly employed for the source apportionment with those offline and online VOCs data sets. In addition, the WRF-CHEM model was adopted in resolving O_3 sources and conducting sensitivity measurement.

This study focuses on the variations of atmospheric VOCs and O_3, which are aimed (1) to obtain characteristics and source apportionment of VOCs in Luoyang and (2) to further investigate the O_3 source attribution and formation sensitivity based on the WRF-CHEM model with the localized data in Luoyang. This paper is organized as follows. Section 2 describes the detailed methodology in VOC measurement and model configuration. Section 3 shows the discussion on the results, including temporal and spatial distributions of VOCs and their source apportionment, source attribution of O_3, and O_3 sensitivity in Luoyang. A brief conclusion is presented in Section 4.

2. Methodology

2.1. Offline sampling collection and analysis

Nine sampling sites of which five and four belongs to urban and suburban, respectively, were selected in this study (Fig. 1). Their locations are representatives to the regions, where were far away from obvious pollution sources. One-hour integrated sample was collected at four time-intervals (i.e., 08:00–09:00, 15:00–16.:00, 18:00–19:00 and 23:00–00:00 LT) in each sampling day between 7th June 2019 and 13th June 2019.

Ambient air was collected onto a stainless-steel multi-beds tube filled with Tenax-TA, Carbograph 1-TD, and Carboxen 1003 (C3-DXXX-5266, Markes International Ltd., Llantrisant, UK) using a low-flow module pump (ACTI-VOC, Markes International Ltd.) at a flowrate of 50 mL min^{-1} for 60 min. No breakthrough was observed under the given flowrate and loading. The sampling inlet was set 1 m above the rooftop which were at the same building of National Air Quality Monitoring Station of China. A disposal Teflon filter and potassium iodide (KI)-coated copper tube were installed in the air upstream to remove any influences from particulate matters and O_3, respectively. One-tenth of parallel sampling were conducted to evaluate the precisions of sampling method. All of the absorbent tube samples were properly shipped and stored in the laboratory before analysis.

The absorbent tubes were analyzed using a thermal desorption (TD) unit (Series 2 UNITY-xr system, Markes International Ltd.) coupled with a gas chromatograph (GC)/flame ionization detector (FID)/mass spectrometric detector (MSD) (Models 7890A/5977B, Agilent, Santa Clara, CA, USA). Certified Photochemical Assessment Monitoring Stations (PAMS) standard gas mixtures (Restek Corporation, Bellefonte, PA, USA) were used for the calibrations. A multipoint calibration curve was established to quantify each target compound with a linearity of $>$ 0.999. The minimum detection limits (MDLs) for the 57 PAMS VOCs analytes were in the range of 0.008–0.326 ppbv with a sampling volume of 3 L (Table S1). The measurement precisions for the analysis of eight replicates of standard samples at 2 ppbv was $\leq$ 5%. Duplicate samples showed the reproducibility was $>$ 95%. Additional details on sampling and analytical methods were described in Section S1.

2.2. Other gaseous measurements

The hourly near-surface NO_x and O_3 concentrations in Luoyang city were monitored using Thermo Scientific™ Model 49i and Thermo Scientific™ Model 42, respectively, which were managed by the National or Provincial Air Quality Monitoring Station of China. The nine sampling sites were selected for offline VOC sampling, where NO_x and O_3 data were available (Fig. 1). The open data (from June 7 to August 10, 2019) and QA/QC information can be downloaded in the official website of http://www.aqistudy.cn/. All the concentrations of the gases were consistently reported in volume-base unit (i.e., ppbv).

2.3. Online measurement

An online VOC monitoring system (TH-300B, Tianhong Inc., Wuhan, China) was employed for continuous measurements of VOCs in an urban site (Jianxi-west) of Luoyang from July 6 to August 10, 2019. This sampling site was representative for urban areas of Luoyang. The instrument consisted of an ultralow-temperature pre-concentrator and a GC/FID/MSD, which was set up 1 m above a five-story height rooftop. The sampling flowrate was set as 60 mL min^{-1}, and the time resolution of each data point was 5 min. A complete working cycle of the online system includes five steps, including (i) sample collection, (ii) cryo-

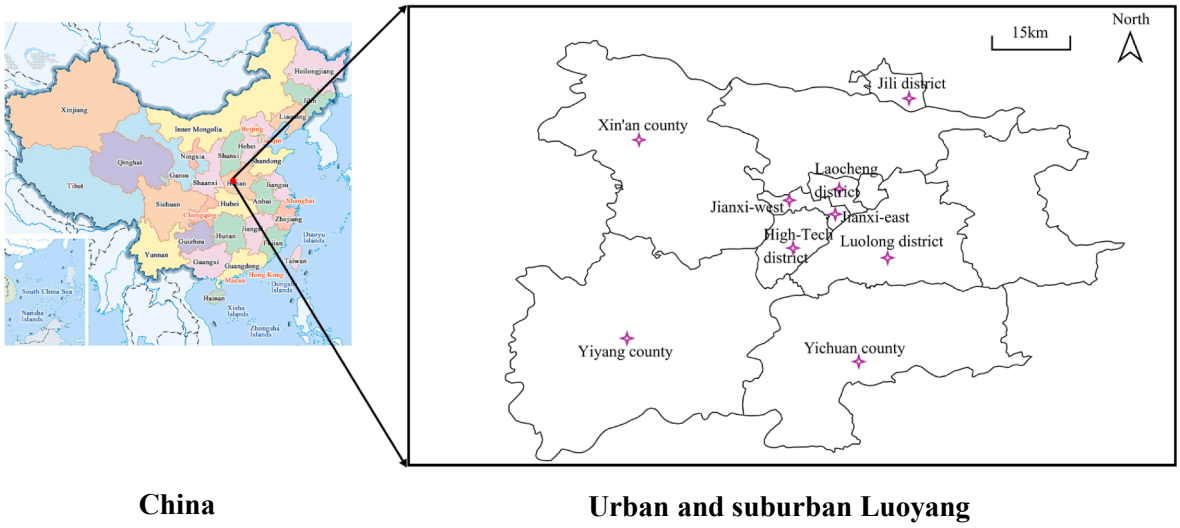

Fig. 1. Maps show the nine sampling sites selected in Luoyang in this study (five urban sites, including Jianxi-west district (JXW), Jianxi-east district (JXE), Laocheng district (LC), Luolong district (LL) and and High-tech district (HT); and four suburban sites, Yichuan county (YC), Yiyang county (YY), Xin'an county (XA), and Jili District (JL).

trapping, (iii) TD releases of analytes, (iv) quantifications by GC/FID/MSD, and (v) heating and anti-blowing purification. Fifty-seven PAMS VOCs were quantified, consistent to those quantified by the offline method. The detailed working flow and instrumental parameters were shown in Section S2.

2.4. Source apportionment of VOCs by HERM

HERM is built upon the ME-2 (multilinear engine) solution to EV-CMB (effective variance Chemical Mass Balance) problems, but differs from the current CMB software (i.e., U.S.EPA CMB v8.2). The model shows ability to analyze one or multiple samples in a single run, inherit non-negativity constraints, and tolerate to collinearity. HERM could also solve profiles that are not assigned a priori or some species that are missing in the profiles and the priority of it compared with EV-CMB and ME-2. Further information about the algorithms of HERM was shown in Section S3. While HERM was being ran, five fixed profiles with the 57 PAMS VOCs were selected as data input (Table 1).

2.5. WRF-CHEM model

A special version of regional WRF-CHEM model (Version 3.5.1) was used to investigate the O_3 formation and source attributions in North China Plain and Luoyang city during the study period (Li et al., 2011, 2012, 2010). The calculation using the WRF-CHEM model accounted multiple parameters, including dynamical inputs (i.e. winds, temperature, clouds and boundary layer), transport (i.e. advection, convection and diffusion), dry deposition (Wesely, 2007), wet deposition, gas-phase chemistry, radiation, and photolysis rates (Tie et al., 2007). Besides, the WRF-CHEM model used in this study contained the following physical schemes in calculation, namely the Goddard longwave and shortwave radiation parameterization (Dudhia, 1989), the WSM 6-class graupel microphysics scheme (Hong and Lim, 2006), the Mellor-Yamada-Janji (MYJ) turbulent kinetic energy (TKE) planetary boundary layer (PBL) scheme (Janić, 2001), the unified Noah land-surface model (Chen and Dudhia, 2001) and Monin-Obukhov surface layer scheme (Janić, 2001). The chemical scheme (CHEM) coupled with WRF in this study is a version of Grell et al. (2005), modified by Tie et al. (2007), and further developed by Li et al. (2010); (2011; 2012;). This specific model includes a new and flexible gas-phase chemical module and the Models-3 community multi-scale air quality (CMAQ, version 4.6) aerosol module developed by the U.S.EPA (Binkowski and Roselle, 2003). Detailed information on the WRF-CHEM model can be found in elsewhere (Li et al., 2011, 2012, 2010).

A high O_3 pollution episode occurred in Luoyang between July 21 and July 27, 2019 was simulated using the WRF-CHEM model. The model adopts one grid with horizontal resolution of 10 km and 35 sigma levels in the vertical direction, and the grid cells used for the domain are 350 × 350 (Fig. 2). The anthropogenic emissions were obtained from the Multi-resolution Emission Inventory of China (MEIC) developed by Zhang et al. (2009), including five sectors of agriculture, industry, power generation, residential and transportation. The National Centers for Environmental Prediction (NCEP) reanalysis data were used to obtain the meteorological initial and boundary conditions. The chemical initial and lateral boundary conditions in the WRF-Chem modeling were created from the global chemical model outputs. The model outputs from MOZART (Model for Ozone and Related chemical Tracers, Version 4) provided by the UCAR/NCAR (Nation Center for Atmospheric Research and University Corporation for Atmospheric Research) are available in different time periods. These have widely been used in previous studies for chemical initial and boundary conditions of regional chemical transportation model simulations (Feng et al., 2018; Le et al., 2020; Wu et al., 2020).

In order to further learn the formation process during the high O_3 concentration level period in Luoyang, a fine-grid simulation was performed using the WRF-CHEM model as well. The center point of the model simulation area was 112.10°E, 34.25°N, while the simulation area grid was 150 × 150 with a resolution of 2 km. Chemical initial and boundary conditions were obtained from the output of the above large-scale simulation. The SAPRC-99 chemical mechanism (Statewide Air Pollution Research Center, version 1999) was employed for the simulation of VOCs and NO_2 in the gas-phase atmospheric reactions (Zhang et al., 2009). The emission inventory used in the WRF-CHEM model was collected from the pollutant emission survey data provided by the Environmental Protection Department of Luoyang City in 2018. It has been standardized by the framework of mosaic inventory provided by MIX (an Asian anthropogenic emission inventory to support Model Inter-Comparison Study for Asia and the Task Force on Hemispheric Transport of Air Pollution). The emission inventory covers five sources including electricity, industry, traffic, agriculture, and residential emissions (Li et al., 2017a). Biogenic sources were quantified using the online MEGAN (Model of Emissions of Gases and Aerosol from Nature, version 2.0) (Guenther et al., 2006). Details of the model configurations are given in Table S2. The simulation domain is shown in Fig. 2.

Table 1
Source profile information used and outputted in HERM (%).

	Gasoline vehicle [1]		Diesel vehicle [2]		Industrial coal [3]		Solvent usage [4]		Petrochemical industry [4]		HERM output-1		HERM output-2	
	MEAN	S.D.	MEAN	S.D.	MEAN	S.D.	MEAN	S.D.	MEAN	S.D.	MEAN	S.D.	MEAN	S.D.
Ethane	3.59	0.75	0.29	0.05	17.57	7.98	n.a.	n.a.	6.21	1.07	8.09	2.62	12.65	2.50
Propane	0.37	0.05	0.84	0.65	6.67	4.10	0.07	0.01	15.89	2.74	19.36	2.62	9.95	1.12
i-Butane	0.53	0.02	0.01	0.01	n.a.	n.a.	0.05	0.01	5.61	0.97	0.75	0.37	1.17	0.25
n-Butane	1.25	0.16	0.01	0.01	0.63	0.66	0.07	0.01	9.04	1.56	0.80	0.12	1.25	0.08
Cyclopentane	0.22	0.05	0.01	0.01	n.a.	n.a.	0.09	0.03	0.73	0.13	0.02	0.01	0.04	0.00
i-Pentane	6.95	0.83	0.89	0.84	1.11	0.51	0.07	0.02	3.20	0.55	0.59	0.22	0.92	0.15
n-Pentane	1.21	0.14	0.01	0.00	1.39	1.41	0.05	0.03	5.09	0.88	0.19	0.06	0.30	0.04
Methylcyclopentane	0.65	0.07	0.01	0.00	0.27	0.21	0.09	0.03	0.91	0.16	0.02	0.02	0.02	0.01
Cyclohexane	0.87	0.10	0.01	0.00	0.13	0.11	0.07	0.03	0.42	0.08	0.00	0.00	0.00	0.00
2,2-Dimethylbutane	0.02	0.02	0.01	0.01	n.a.	n.a.	0.00	0.00	0.14	0.03	0.04	0.01	0.06	0.01
2,3-Dimethylbutane	0.01	0.01	0.02	0.01	0.12	0.16	0.19	0.06	0.19	0.04	0.05	0.02	0.07	0.01
2-Methylpentane	3.33	0.04	0.02	0.03	0.61	0.56	0.87	0.33	1.90	0.33	0.08	0.02	0.12	0.01
3-Methylpentane	1.63	0.15	0.00	0.00	0.19	0.17	0.72	0.29	3.30	0.57	0.07	0.02	0.11	0.01
n-Hexane	1.02	0.13	0.20	0.19	1.02	0.92	1.26	0.46	3.12	0.54	0.25	0.04	0.40	0.03
Methylcyclohexane	0.45	0.03	0.01	0.00	0.09	0.10	0.14	0.04	0.72	0.13	0.01	0.01	0.02	0.00
2,3-DimethylPentane	0.46	0.05	0.01	0.00	0.33	0.35	0.00	0.00	0.35	0.06	0.01	0.01	0.02	0.00
2,4-Dimethylpentane	0.34	0.02	0.02	0.03	n.a.	n.a.	n.a.	n.a.	0.05	0.01	0.01	0.01	0.01	0.01
2-Methylhexane	1.70	0.37	0.02	0.01	0.13	0.19	0.07	0.02	0.49	0.09	0.19	0.07	0.30	0.05
3-Methylhexane	1.74	0.34	0.01	0.00	n.a.	n.a.	0.09	0.02	0.64	0.11	0.07	0.02	0.11	0.01
n-Heptane	0.75	0.03	0.77	0.66	1.22	0.72	0.24	0.06	1.85	0.32	0.08	0.01	0.13	0.01
2,2,4-Trimethylpentane	0.61	0.08	0.01	0.00	n.a.	n.a.	n.a.	n.a.	0.01	0.00	0.04	0.00	0.07	0.00
2,3,4-Trimethylpentane	0.48	0.06	0.01	0.00	n.a.	n.a.	n.a.	n.a.	0.03	0.01	0.01	0.01	0.02	0.00
2-Methylheptane	1.06	0.17	0.01	0.00	0.49	0.25	0.20	0.06	0.27	0.05	0.02	0.01	0.03	0.00
3-Methylheptane	0.94	0.09	0.01	0.00	0.18	0.11	0.09	0.02	0.09	0.02	0.02	0.01	0.03	0.00
n-Octane	0.26	0.04	0.01	0.00	0.86	0.41	1.01	0.23	0.66	0.12	0.09	0.06	0.14	0.04
n-Nonane	0.21	0.02	0.01	0.00	0.50	0.44	1.41	0.41	0.17	0.03	0.02	0.02	0.03	0.01
n-Decane	0.24	0.04	0.74	0.36	0.56	0.20	0.82	0.39	0.08	0.02	0.04	0.06	0.07	0.04
n-Un.a.ecane	0.22	0.02	8.33	2.20	0.54	0.18	0.19	0.09	0.07	0.01	0.02	0.01	0.04	0.01
Ethene	12.36	1.03	16.47	2.95	13.22	7.89	n.a.	n.a.	8.18	1.41	18.14	4.77	12.73	3.24
Propene	4.92	0.63	0.01	0.01	9.29	1.42	0.02	0.00	12.82	2.21	4.28	1.52	6.70	1.04
1,3-butadiene	0.92	0.07	n.a.	n.a.	n.a.	n.a.	n.a.	n.a.	0.03	0.01	0.32	0.09	0.51	0.06
1-Butene	2.28	0.13	1.46	1.04	1.53	0.88	0.00	0.00	3.63	0.63	1.18	0.25	1.84	0.17
cis-2-Butene	0.31	0.03	0.01	0.01	1.93	1.59	n.a.	n.a.	0.63	0.11	0.25	0.05	0.39	0.03
trans-2-Butene	0.38	0.03	0.02	0.02	1.07	0.61	n.a.	n.a.	0.69	0.12	0.36	0.11	0.57	0.07
Isoprene	0.31	0.08	2.35	2.21	n.a.	n.a.	0.02	0.01	0.02	0.00	0.49	0.11	31.93	4.99
1-Pentene	0.26	0.06	0.01	0.01	0.75	0.51	n.a.	n.a.	1.37	0.24	0.12	0.04	0.19	0.02
cis-2-Pentene	0.21	0.02	0.01	0.00	0.09	0.13	n.a.	n.a.	0.16	0.03	0.03	0.01	0.05	0.01
trans-2-Pentene	0.13	0.02	0.01	0.00	0.07	0.10	n.a.	n.a.	0.35	0.06	0.03	0.01	0.05	0.01
1-Hexene	0.20	0.02	0.03	0.02	0.56	0.40	n.a.	n.a.	1.42	0.25	0.06	0.02	0.09	0.01
Ethyne	5.08	1.19	5.17	0.93	6.32	1.13	n.a.	n.a.	0.95	0.17	27.89	1.41	12.35	0.96
Benzene	9.25	0.81	0.01	0.00	16.98	5.47	0.46	0.13	3.27	0.57	10.27	1.79	0.43	1.22
Toluene	11.80	0.66	4.89	2.44	7.66	1.28	13.99	2.04	3.50	0.60	3.68	0.49	1.06	0.33
m/p-Xylene	0.21	0.01	3.74	1.56	2.33	0.13	13.77	1.02	0.49	0.09	0.49	0.20	0.77	0.13
Ethylbenzene	1.63	0.38	3.27	1.32	0.93	0.14	27.80	2.14	0.66	0.12	0.33	0.11	0.52	0.07
o-Xylene	n.a.	n.a.	4.81	1.67	0.83	0.11	7.89	0.54	0.18	0.03	0.20	0.09	0.31	0.06
Styrene	0.56	0.08	13.09	7.54	0.05	0.03	12.66	2.52	0.05	0.01	0.33	0.06	0.52	0.04
1,2,3-Trimethylbenzene	2.27	0.22	1.32	0.32	0.23	0.06	1.01	0.22	0.03	0.01	0.06	0.04	0.09	0.03
1,2,4-Trimethylbenzene	4.07	0.26	5.05	2.03	0.38	0.07	1.89	0.35	0.08	0.02	0.09	0.05	0.14	0.03
1,3,5-Trimethylbenzene	0.40	0.02	0.17	0.08	0.13	0.02	0.89	0.20	0.02	0.00	0.06	0.04	0.10	0.03
i-Propylbenzene	0.57	0.14	4.03	1.97	0.02	0.03	2.85	0.48	0.01	0.00	0.02	0.01	0.04	0.00
m-Ethyltoluene	1.24	0.13	0.01	0.00	0.30	0.03	5.25	1.12	0.06	0.02	0.10	0.05	0.16	0.03
n-Propylbenzene	0.35	0.03	12.48	7.49	0.08	0.07	n.a.	n.a.	0.03	0.01	0.03	0.01	0.05	0.00
o-Ethyltoluene	1.15	0.24	6.09	3.85	0.15	0.04	1.14	0.24	0.04	0.01	0.05	0.03	0.08	0.02
p-Ethyltoluene	2.19	0.12	0.01	0.00	0.13	0.02	1.98	0.43	0.03	0.01	0.05	0.02	0.08	0.02
m-Diethylbenzene	1.39	0.15	2.29	1.92	0.09	0.12	0.12	0.03	0.01	0.00	0.11	0.27	0.17	0.18
p-Diethylbenzene	4.43	0.89	0.83	0.85	0.26	0.09	0.44	0.11	0.02	0.01	0.01	0.01	0.02	0.01

n.a. denotes not detected or below detection limit.
1. Wang et al., 2013; 2. Tsai et al., 2012; 3. Liu et al., 2008; 4. This study.

2.6. Statistical methods for comparisons

Mean bias (MB), root mean square error (RMSE) and the index of agreement (IOA) were used to assess the WRF-CHEM model veracity in simulating air pollutants against measurements with the equations of:

$$MB = \frac{1}{N}\sum_{i=1}^{N}(P_i - O_i) \quad \text{(i)}$$

$$RMSE = \left[\frac{1}{N}\sum_{i=1}^{N}(P_i - O_i)^2\right]^{\frac{1}{2}} \quad \text{(ii)}$$

$$IOA = 1 - \frac{\sum_{i=1}^{N}(P_i - O_i)^2}{\sum_{i=1}^{N}(|P_i - \overline{O}| + |O_i - \overline{O}|)^2} \quad \text{(iii)}$$

where P_i and O_i are the calculated and observed pollutant concentrations, respectively, N is the total number of the predictions used for comparisons, and $\bar{o}$ are the averages of the prediction and observation, respectively. The IOA ranged from 0 to 1 in the calculation. The IOA more approaching to 1 represents a higher agreement between the prediction and observation values.

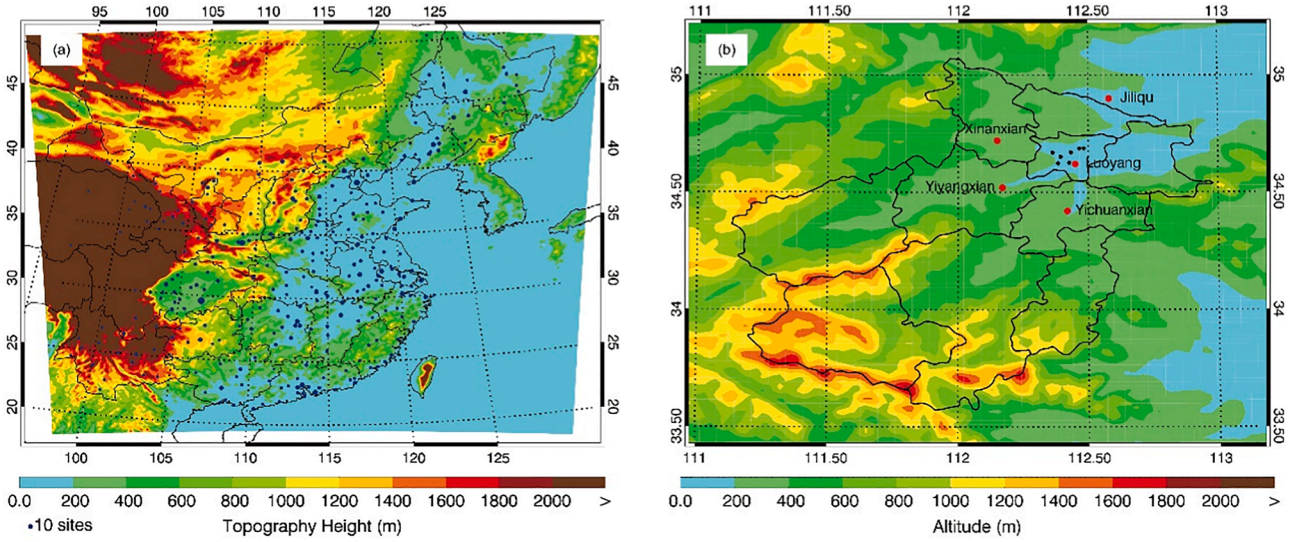

Fig. 2. WRF-CHEM simulation domain with topography. The filled circles represent centers of cities with ambient monitoring sites, and the size of circles denotes the number of ambient monitoring sites of cities. The red and blue filled circles show the cities with air pollutant observations since 2013 and 2015, respectively. (a) Simulation domain of eastern China; (b) simulation domain of Luoyang city. (For interpretation of the references to color in this figure legend, the reader is referred to the web version of this article.)

3. Results and discussion

3.1. Spatial and temporal distribution of PAMS VOCs in Luoyang

The average mixing ratios of 57 PAMS VOCs, O_3, and NO_x at the sampling sites are illustrated in Fig. 3. Obvious spatial distribution was seen between the urban and suburban areas. For the five urban sites, the total PAMS VOCs (TVOCs) concentrations ranged from 14.5 ± 5.33 ppbv (Luolong district) to 29.2 ± 11.2 ppbv (Laocheng district). The distance between the highest and lowest sites was less than 10 km, but their concentration differences showed a factor of two. In comparison, the urban sites of Laocheng and Jianxi-west districts with relatively higher TVOC concentrations had common characteristics. These two sites were classified as old towns, located at downwind, and had high population and traffic densities. For the suburban, the spatial differences were even much obvious than those observed in the urban. The highest TVOC concentration of 37.6 ± 14.0 ppbv was observed in Jili district where many petroleum-industries were found and was far away from the downtown Luoyang. The lowest level was seen in Yichuan county, with an average concentration of 12.0 ± 4.36 ppbv. Correspondingly, lower NO_x concentrations were seen at the suburban sites (18.2 ± 5.17 ppbv on average) than the urban sites (27.2 ± 3.32 ppbv on average). However, the O_3 concentrations did not show good correlations between the precursors of TVOC and NO_x at the nine sampling sites. The spatial distribution of O_3 were also inconsistent to the values of ozone formation potentials (OFP) (calculation method was described in Section S4) calculated at each site (Table S3). These represent that the study of the O_3 sensitivity is important in Luoyang city.

Intensive temporal variation was demonstrated with the online measurement. Fig. S1 shows the time series of the concentrations of TVOCs, NO_x and O_3 in Jianxi-east district located in urban Luoyang from July 6 to August 9, 2019. The concentrations of VOCs and NO_x ranged from 11.4 to 96.2 ppbv and 4.00 to 102 ppbv, respectively, while an average 8-hour O_3 concentration of 137.8 ± 34.9 μg m^{-3} was seen throughout the monitoring period. The diurnal variations of the TVOCs and NO_x were similar but were reversible with O_3. Such observations are

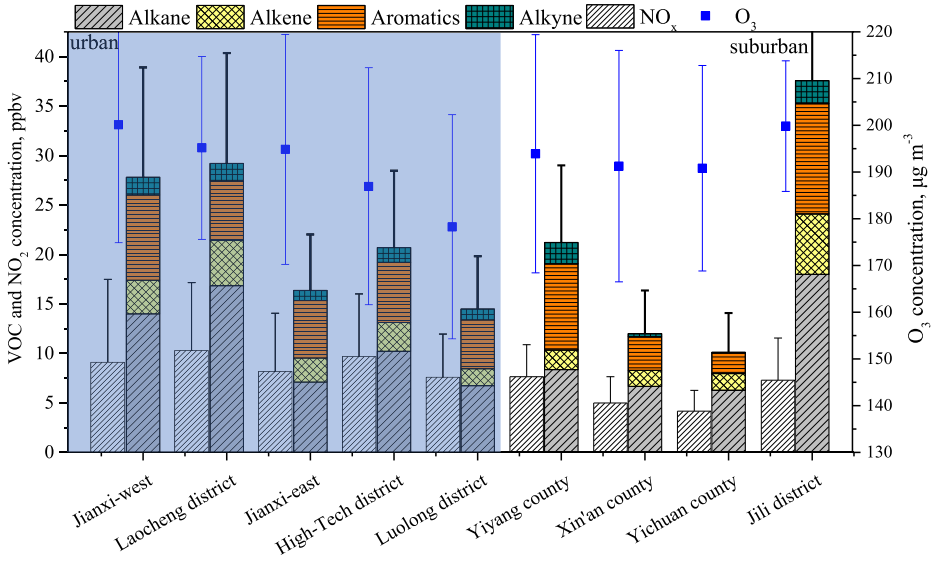

Fig. 3. The average mixing ratios of PAMS VOCs (ppbv) in nine sampling sites measured with offline method.

consistent with those reported in the literature (Hui et al., 2018). The daily average VOC concentrations and their composition were compared with those measured in other Chinese megacities (Fig. S2). As the smallest scale among the six megacities, Luoyang showed moderate level of TVOCs (20.9 ± 10.3 ppbv) which was slightly lower than those in Guangzhou (27.0 ± 14.9 ppbv) and Shanghai (23.8 ± 14.7 ppbv) ($p > 0.05$), and comparable with those in Beijing (22.5 ± 12.8 ppbv) and Wuhan (21.7 ± 18.9 ppbv) (Huang et al., 2017; Hui et al., 2020; Liu et al., 2019; Wei et al., 2018). It is worth noting that the average TVOC concentration in Luoyang was even higher than that in Xi'an (19.0 ± 18.9 ppbv) (Sun et al., 2019). Considering that Xi'an was only ~ 300 km away from Luoyang and had a higher population size and numbers of vehicles and industries, the poor diffusion condition in Luoyang would be a possible reason for the high VOC levels. Regarding to VOC chemical fractions, a unique finding is that the proportion of alkanes in Luoyang was ~ 50% of TVOCs which was much lower than that in the other cities (62%–70%) (Gu et al., 2019; Liu et al., 2019). Accordingly, the proportions of alkenes and alkyne were relatively high. This feature could reflect the characteristics of the energy structure in Luoyang where petrochemical industries and coal combustion (both emit large proportion of alkenes and alkyne) are predominant (An et al., 2012). It also elucidated that the high O_3 concentrations in Luoyang could be resulted from the high photochemical activities of alkenes and alkyne (Shao et al., 2016).

Fig. 4 shows statistical hourly-average variations of VOCs, NO_x and O_3 in nine sampling sites of Luoyang. As mentioned above, the diurnal patterns of VOCs and NO_x were similar ($R^2 = 0.80$, $p < 0.05$) but reverse with O_3 (R^2 = -0.63 and −0.46 for VOCs and NO_x, $p < 0.05$). It could be simply explained by the fact that both VOCs and NO_x are crucial precursors for the O_3 production (Pollack et al., 2012; Wang et al., 2017b). In addition, ambient VOCs can lead to the formation of peroxy radical ($RO_2^{\bullet}$) which is further disrupted the dynamic balance of NO–O_3–NO_2 reactions (Hui et al., 2020). This also leaded relatively weak correlations between O_3 and NO_x. On the other hand, similar diurnal variations of TVOCs were seen among the monitoring period (Table S4), with the lowest and highest concentrations at 14:00–15:00 LT and 08:00–09:00 LT, respectively. The pattern was closely associated with photochemical reaction processes, meteorological conditions and emission sources (Hui et al., 2020). Obvious increases of TVOCs (especially for aromatics and alkyne) and NO_x were showed at 04:00–05:00 LT. This could be explained by the emissions from vehicles (e.g., heavy-duty trucks) at nighttime or before dawn. Alkenes, alkyne and aromatics all showed over 100% diurnal variations (max/min), much higher than that of alkanes which had the lowest photochemical activities (Kumar et al., 2018). An exception was observed for isoprene which is a well-known biogenic VOC (BVOC). The concentrations of isoprene were much higher in the daytime than nighttime, correlated with both ambient temperature and light intensity. This reflected the characteristic of BVOC emissions (Mo et al., 2018). Diurnal PBL variation is a non-negligible factor in influencing diurnal pattern of VOCs, NO_x and O_3 despite in different modes (Ding et al., 2008). In detail, the enhancement of PBL in the afternoon was a crucial parameter for the decreases of NO_x and VOCs. In comparison, due to the vertical distribution of O_3 in troposphere, higher concentrations of O_3 in upper troposphere could contribute to the surface O_3 in the afternoon, when the peak O_3 level was seen during 15:00–18:00 (LT) with relatively stronger photochemical reactions and regional transportation than other time intervals (Gaudel et al., 2018).

3.2. VOC source apportionment

Five VOCs source profiles, including gasoline vehicle emission, diesel vehicle emission, industrial coal combustion, solvent usage and petrochemical industry, were obtained from literatures (Liu et al., 2008a; Tsai et al., 2012; Wang et al., 2013). The data collected from the field measurement (i.e., 57 PAMS VOCs shown in Table 1) was input in the HERM model and a sampling survey was conducted to verify the representativeness of the source profiles in literature. Cases with Q value (reproduction of the number of degrees of freedom in calculation) over 1000 and a $R^2 > 0.80$ were kept for further calculation after several trials of iterative operation. Two profiles with uncertainties (namely Output-1 and Output-2) were generated by the HERM calculation. The HERM Output-1 showed high abundances of propane, ethene, ethyne and benzene, conforming the features of coals and natural gas combustions and thus being identified as residential combustion source (An et al., 2017; Zhang et al., 2016). For the HERM Output-2, it was dominated with dramatically high abundances of isoprene and short-chain hydrocarbons, and thus acknowledged as biogenic source (Kelly et al., 2018;

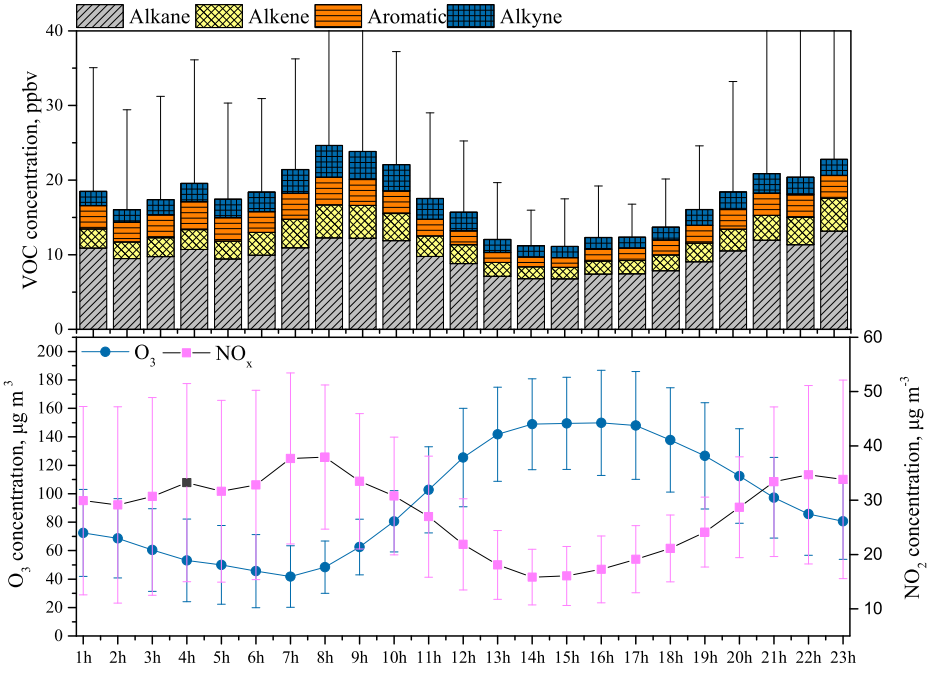

Fig. 4. Statistical hourly-average concentration variations of VOCs, NO_x and O_3 of nine monitoring station in Luoyang.

Kleindienst et al., 2007).

The source apportionment results in urban and suburban are shown in Fig. 5. The seven sources were identified in both urban and suburban but showed quite different distributions among the regions. Industry (expressed as the sum of petrochemical industry, solvent and industrial coal combustion) and traffic (expressed as the sum of gasoline and diesel vehicle emissions) were the two most dominant VOCs sources in Luoyang, with a total contribution of > 70%. Higher contributions of traffic were found in urban (32.0%) than suburban (20.9%), but a reverse phenomenon was seen for industry with the contributions of 38.5% and 50.1% for urban and suburban, respectively. It is understandable that the vehicle density in urban were much higher than that in suburban (Kumar et al., 2018; Zhang et al., 2016). Besides, according to the figures shown in the Luoyang's Statistical Year Book 2018 (LBS, 2018), the industries were majorly located in suburban, hypothetically explained the higher contribution of the industrial source than urban. An extreme case was seen in Jili district where the contribution of petrochemical industry was as high as 40.2% (Fig. S3). Many petrochemical plants located within the district and produced chemical products which have been converted from natural resources such as petroleum or crude oil. The contributions of residential sources were slightly higher in urban (13.8%) than suburban (10.0%), attributed with the higher population density in the city center. For biogenic source, it is not surprise that higher contribution was seen in suburban (19.0%) than urban (15.8%). For the countryside site of Yiyang county, the contribution of biogenic source was even high as 35.4% that could be explained by the strong input of vegetation to some extent (Fig. S3).

The consistency of the source apportionments with the data collected by the online- and offline-based VOCs measurements was accessed at Jianxi-east district. In general, good agreements on the source contributions were obtained between the two sets of data (Fig. 5). The offline-based method showed a slightly lower contributions of residential sources (9.4%) than the online method (13.5%). However, higher contribution of biogenic source was showed in offline (10.8%) than online (5.1%) methods. It should be noted that the samples collected by the offline method were time-selective (i.e., four time-interval a day), potentially not reflecting the entire residential emission strength (e.g., without accounting the cooking emission during lunch time) (Lee et al., 2002). In addition, most of the offline samples were collected at daytime, thus the contributions of biogenic sources might be overestimated due to their diurnal emission characteristics (Li et al., 2018a; Mo et al., 2018). The contributions of industrial and transportation sources between the two methods were comparable, suggesting that the time-selective offline sampling was adoptable and effective to account their contributions.

3.3. WRF-CHEM model performance

In order to examine the accuracy of stimulations using the WRF-CHEM model, the results were compared with the hourly measurement of O_3 and NO_2 in the central-eastern China and Luoyang City (shown in Fig. S4 and Fig. 6, respectively). The average geopotential height wind filed at 500 hPa from July 21 to 27, 2019 (Fig. S4) that illustrated the effects of the meteorological conditions on the air quality. Generally, most areas in the central-eastern China (including NCP and eastern China) were located behind the trough and with center at 130 °E. During the study period, the central-eastern China was mainly controlled by the subtropical high at 500 hPa located in the western

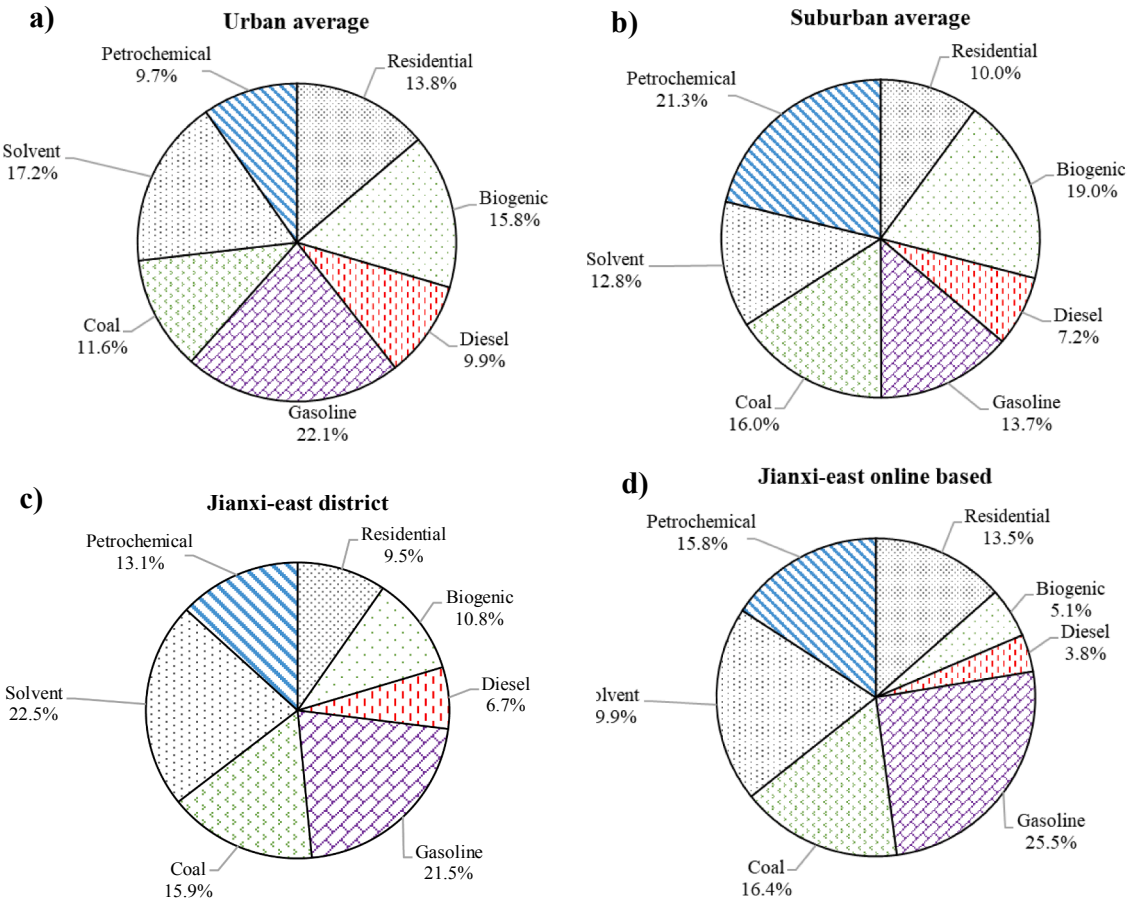

Fig. 5. VOC source apportionment results for (a) urban average with offline data, (b) suburban average with offline data, (c) Jianxi-east with offline data and (d) Jianxi-east with online data.

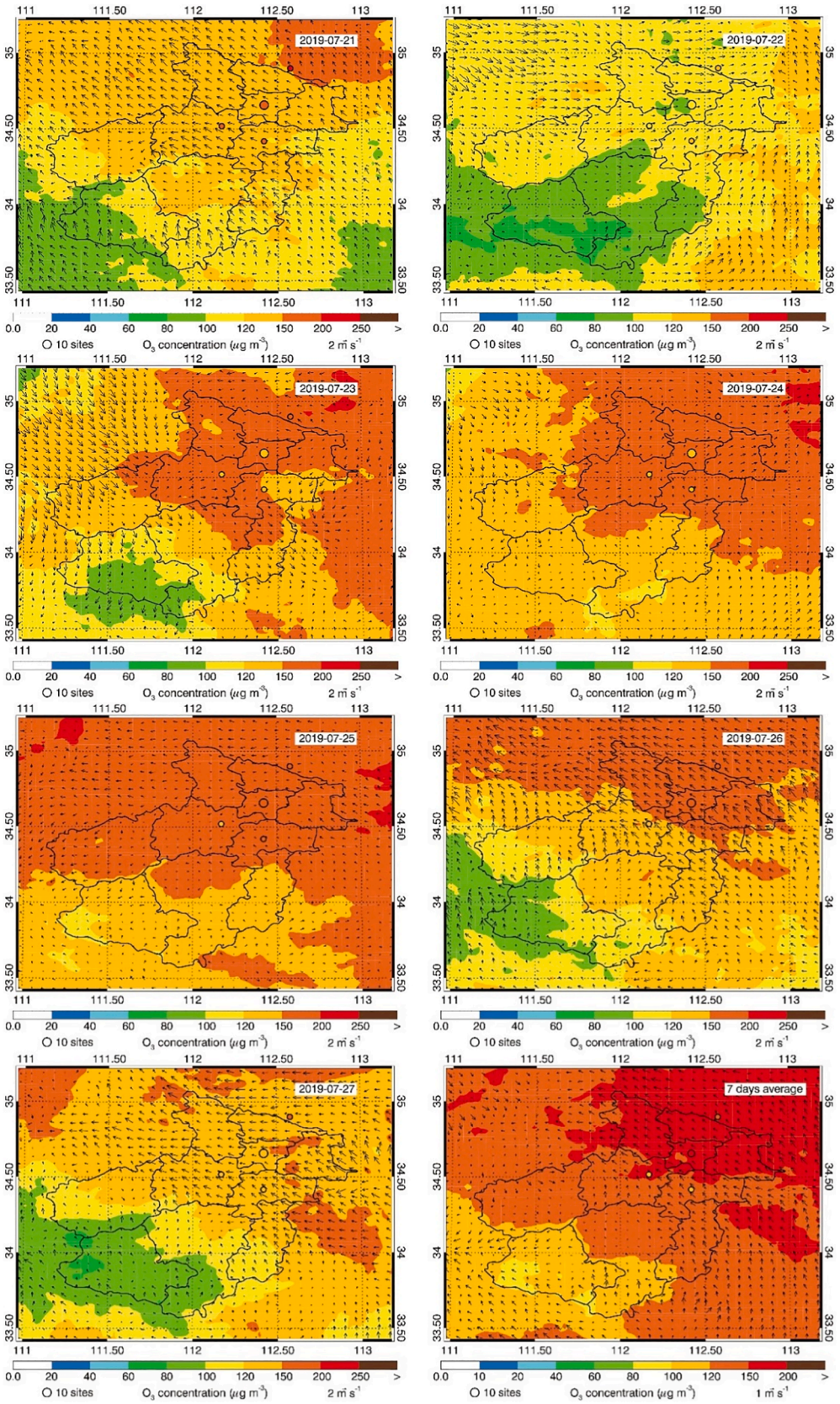

Fig. 6. Pattern comparison of simulated versus observed near-surface O_3 at Luoyang from July 21 to July 27, 2019. (Colored circles: O_3 observations; color contour: O_3 simulations; black arrows: simulated surface winds) (Data of five urban stations were merged together as a large dot with average data; three suburban stations were used excluding Xin'an county due to data validation).

Pacific, leading to prevailing wind directions of south and south-east. As shown in Fig. S4, the maximum 8-h average concentrations of O_3 of the NCP were over 100 μg m^{-3}, and even exceeded 160 μg m^{-3} in few areas, reflecting severe regional O_3 pollution. Fig. S5 illustrates the diurnal trends of the averages of calculated and observed near-surface O_3 concentrations at the ambient monitoring sites in the related provinces and municipalities in the North China Plain during the episode periods. The O_3 concentrations on July 21–22 were underestimated due to the influence of initial boundary conditions. A small overestimation of O_3 concentrations was shown in the morning of July 24–27, possibly attributed to the underestimation of NO_2 emissions in the rush hours. Averagely, the WRF-CHEM simulation showed good correlations with the observation data, with IOA up to 0.92, MB and RMSE of −4.9 and 22.4 μg m^{-3}, respectively for O_3; and IOA of 0.84, MB and RMSE of −0.2 and 5.6 μg m^{-3} for NO_2. The simulation by the WRF-CHEM model in this work showed comparable and even above average performance than similar studies in NCP and central China (Wang et al., 2019b; Wu et al., 2018a), indicating our application of WRF-CHEM could accurately simulate the diurnal variations of O_3 and NO_2 concentrations in the NCP.

The daily average O_3 concentration was 97.7 μg m^{-3}, ranged from 80 to 150 μg m^{-3}, during the episode period (Fig. 6). The WRF-CHEM model slightly overestimated the O_3 concentrations with an average of 103.2 μg m^{-3}, which mostly occurred in midnight and early morning. This could be ascribed with the high uncertainty in NO_2 emission inventory (also named spatial and temporal disaggregation of the emission inventory) when obvious NO_2 peaks were seen at these two sections (as aforementioned in Section 3.1). This could lead the O_3 depleting has not been well simulated. However, the model obviously underestimated the O_3 peak concentrations in the afternoon on the first episode day (July 21) due to the short spin-up times which may break a integrate meteorological process (Li et al., 2017b). Meteorological conditions were widely reported to play key roles in the formation, transportation, diffusion and removal of O_3 and other air pollutants (Bei et al., 2010, 2012). In this study, the O_3 distribution was highly correlated with wind directions. The downwind areas showed significantly higher O_3 concentrations than upwind areas on specific dates such as July 21, 22 and 27. Extremely low wind speed occurred on July 23–25 promoted the cumulation of O_3, demonstrated by the highest O_3 concentrations (150–200 μg m^{-3}) during the period. Besides of horizontal transportation, vertical contribution of boundary layer O_3 is another potential parameter to the high O_3 concentrations in the afternoon. Without taken account of this factor, it might lead the underestimation of O_3 in the simulation on July 21 (Gaudel et al., 2018). The WRF-CHEM model stimulated the IOA as high as 0.85 and slightly overestimated the observed O_3 concentrations with MB of 5.4 μg m^{-3} and RSME of 37.1 μg m^{-3} (Fig. 7). Besides, the model could reasonably yield the temporal variations of NO_2, with IOA of 0.62, MB and RMSE of −2.7 μg m^{-3} and 15.2 μg m^{-3}, respectively. These performance in city scale simulation were comparably lower than those in the regional simulations especially for NO_2, which is possibly caused by the model biases in estimating the planetary boundary layer (PBL) or unpredicted human activities at nighttime (Li et al., 2017b, 2010). However, the statistical results were still fall into the range in the city-scale literatures (Bocquet et al., 2015; Chen et al., 2013), indicating a satisfied modeling precipitation process of this study.

3.4. Attribution of O_3 sources by WRF

As the importance to establish efficient O_3 control strategies, the sources of O_3 formations from either local emission sources or regional transportations must be defined. The factor separation approach (FSA) was employed to evaluate the contributions. The approach differentiates the O_3 concentrations calculated by two simulation models. One accounted all emission sources and the other accounted without one or multiple sources. Four sensitivity simulations including local, transportation, background and interactions were performed, and their estimated contributions among the study period are shown in Table 2. The results indicated that the external transportation contributed 43.2% (corresponding to 69 μg m^{-3}) on the day with the maximum daily O_3 concentration. In normal days, the local sources had higher contributions (63.6% on average) to O_3 than the transportations in Luoyang. It should be noted that the local sources consisted of both anthropogenic sources and background, with average contributions of 19.4% and 44.2%, respectively. In addition, the interactions between the local and transportation sources would lead a decline of the maximum 8-h average

Table 2
Distribution of local and external transportation to maximum 8-h average O_3 concentration in Luoyang (%).

Date	External transportation	Local contribution	Interaction	Background
07.21	32.5	28.4	–23.4	62.5
07.22	38.2	8.5	−5.8	59.1
07.23	42.6	4.1	−1.3	54.6
07.24	54.0	24.5	−13.2	34.7
07.25	35.3	27.1	−2.9	40.5
07.26	35.2	16.8	6.9	41.1
07.27	60.3	18.9	−8.4	29.2
Period average	43.5	19.4	−7.1	44.2

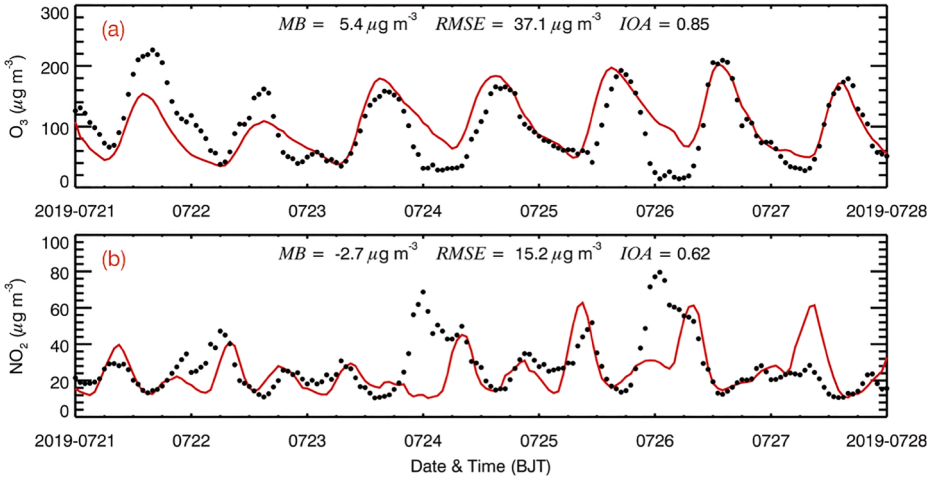

Fig. 7. Comparison of measured (black dots) and predicted (red line) diurnal profiles of near-surface O_3 and NO_2 averaged nine ambient monitoring stations in Luoyang from July 21 to July 27, 2019. (For interpretation of the references to color in this figure legend, the reader is referred to the web version of this article.)

O_3 concentration by 7.1% due to the nonlinear effect on the O_3 formation with VOCs and NO_x (Xing et al., 2011). According to Fig. S5, the transportation contribution to O_3 in Luoyang in the first two days may be slightly overestimated due to initial conditions. The average contribution of transportation in next five days (45.5%) still inferred that sole restriction of local anthropogenic sources was insufficient. The inter-regional prevention and controls would be thus an effective solution. Fig. S6 further presented the spatial contributions of the four identified sources on the maximum 8-h average O_3 concentration in Luoyang. It revealed that 20–40 μg m^{-3} of O_3 was produced by the local emission in the center of the urban area. Besides, the O_3 concentrations in Luoyang was highly influenced by the external transportation from adjoining areas to its east and south during the study period.

Local sources in Luoyang were apportioned. Seven simulations were conducted including one with all six emissions sources (i.e., agricultural, power plant, biogenic, industry, residential, and traffic) and other six

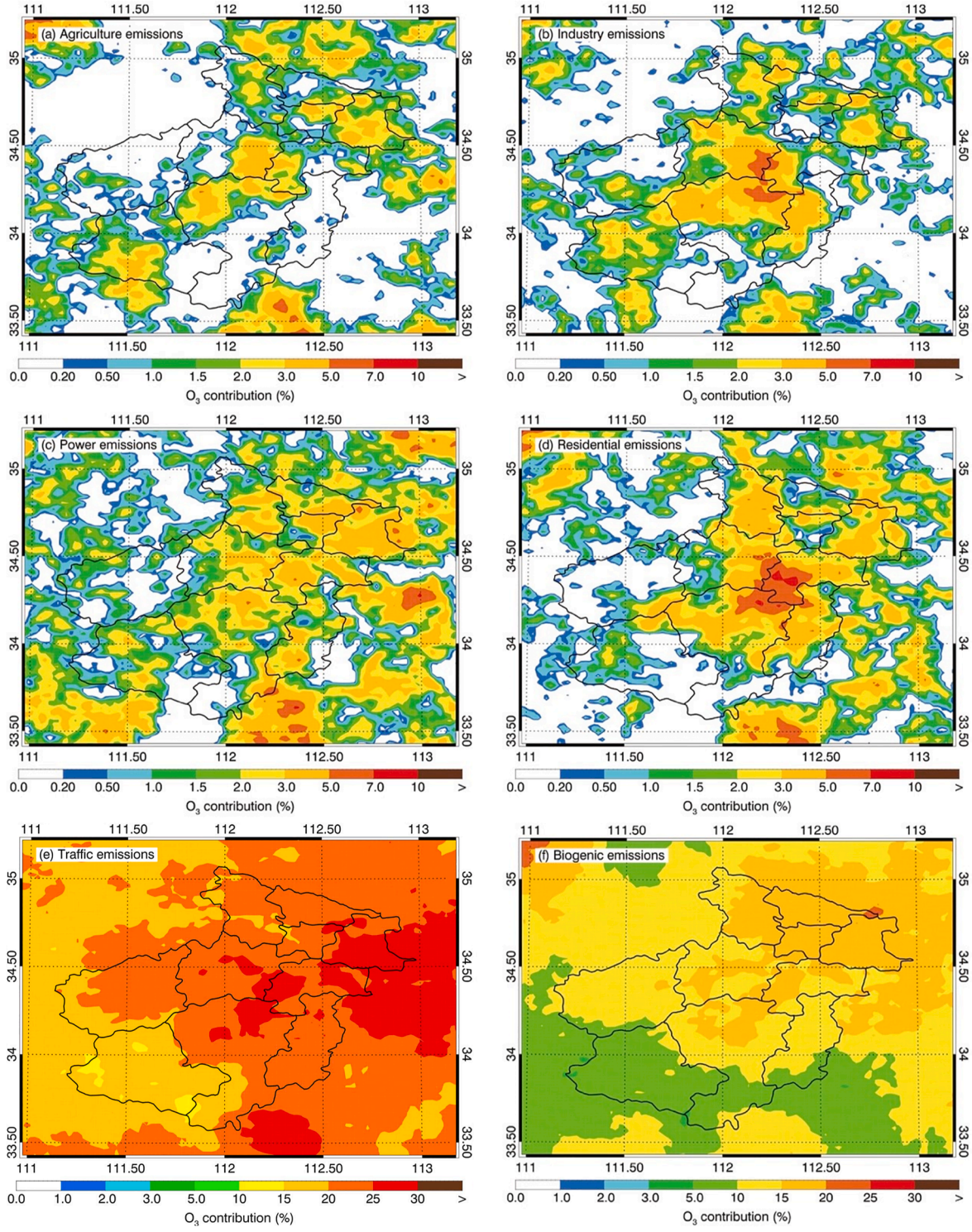

Fig. 8. Distributions of the contribution to near-surface [O_3] (maximum 8-hour sliding average) during the whole episode from (a) agriculture emissions (b) industry (c) power emissions (d) residential emissions (e) traffic emissions and (f) biogenic emissions.

with one source absented in sequence. Fig. 8 shows their contributions on the maximum 8-h average concentration of O_3. Traffic and biogenic sources were the two most important contributors on O_3 in Luoyang, while industrial showed the least contribution. In contrast, the contributions from agricultural source, power plant and residential source were moderate, accounting for less than 10 μg m^{-3} of O_3. Biogenic source acts as natural O_3 precursors and accordingly contributed 28.7 μg m^{-3} of O_3. Unfortunately, biogenic source cannot be artificially controlled (Kleindienst et al., 2007; Li et al., 2018a). The daily and averaged source contributions were summarized in Table 3. The contributions of industrial and power plant were found to be very limited in Luoyang. One possible explanation was that these two sources emitted equivalent amounts of NO_x and VOCs. While they were removed in the simulation, the reduction of O_3 would be offset by each other (Li et al., 2017b). Essentially, the emissions from industrial and power plant sectors were under good control by the local government. In case of both these two sources were removed from the stimulation, the maximum 8-h average O_3 still exceeded 160 μg m^{-3} on the episode days. The traffic emission was the most prominent anthropogenic source with an average contribution of 36.0 μg m^{-3} to O_3 in the afternoon. Considering the rapid growth of numbers of vehicles in China (Wu et al., 2016), traffic emissions would become more critical in the O_3 pollution control (Li et al., 2017a). Apparently, controls of local traffic emissions should be priorly considered when relevant strategies on the prevention and control of O_3 pollution are being established in Luoyang in summertime. It should be noted that the FSA used in O_3 source attributions introduces uncertainties to the simulation results and leads to vagueness in resolving external transportation source. This could be improved with advanced emission tagging method provided by Lupaşcu and Butler (2019) (see Table 4).

3.5. O_3 sensitivity to VOCs and NO_x

As discussed above and shown in literatures, the nonlinear relationship in formation of atmospheric O_3 from VOCs and NO_x often troubled the O_3 simulation control (Feng et al., 2016; Lyu et al., 2016; Verstraeten et al., 2015). Determination of local O_3 formation sensitivity to VOC or NO_x is thus necessary for establish effective O_3 control strategies. In this study, only anthropogenic emissions would be taken into account (referred to the emission inventory of Luoyang in 2019), whereas the biogenic emissions were uncountable. The present emissions of NO_x and VOCs were set as baseline with ratio of 100%. Both NO_x and VOC emission ratios were set 10% as gradient from 100% to 0%, and totally 121 sensitivity simulations were conducted. The O_3 concentration isopleths in the afternoon of summer (i.e., from 12: 00 LT to 19: 00 LT) in Luoyang was shown in Fig. 9. Flex Ratio (FR), defined as NO_x emission ratio when the O_3 concentration reached the maximum value under VOCs baseline, was used to identify the O_3 regime in Luoyang (Xing et al., 2011). When FR is less than 1, the O_3 formation was sensitive to VOCs. FR higher than 2 represents a NO_x-limited regime. In case of FR between 1 and 2, this indicates a transitional regime which the reductions of either NO_x or VOC would be expected to reduce O_3 efficiently (Jin and Holloway, 2015).

As shown in Fig. 9, the FR was 1.0 (indicated by red triangle), representing that the O_3 formation in the atmosphere of Luoyang was in transitional regime and collectively controlled by NO_x and VOCs. In another word, the reductions of local NO_x or VOCs emissions would overwhelm the O_3 concentration in summertime. The isopleths pointed out that the sole reduction of NO_x would not lead the reduction of O_3 concentration until 45% of the NO_x emission being cut down. For VOCs, the O_3 concentration would decline if 70% of their emissions could be reduced. The ridge-line of the isopleths additionally demonstrated that the reduction in accordance with the anthropogenic VOCs (AVOCs) to NO_x mass concentration ratio of 3:1 was the best fit on mitigating O_3 pollution in Luoyang. The sole control of NO_x would be only effective when the O_3 concentrations was controlled below 160 μg m^{-3}, meaning that the O_3 formation was under typical NO_x-limited regime.

Our results did find some differences with those conducted in NCP. Xing et al. (2011) reported that Beijing, Tianjin and Shanghai all exhibited VOCs-limited regime on the O_3 formation in 2005 due to the high levels of NO_x emission. However, the shift of O_3 formation regimes from VOC-limited to NO_x-limited was not only found in our study. Many researches also reported that such transitional regime was occupied over the NCP, Yangtze River Delta (YRD), and the Pearl River Delta (PRD) regions during the high O_3 periods (Jin and Holloway, 2015; Ye et al., 2016). The possible explanation is that the NO_x concentration levels in China sharply decreased since 2013 when the strict control policies were implanted (Wang et al., 2019a). On the base of chemical views, the declines of NO_x could lead increases of ambient HO_x free radicals (i.e., $HO^{\bullet}$, $HO_2^{\bullet}$, $RO_2^{\bullet}$) which further shifted the HO_x loss routine to $HO_2^{\bullet} + RO_2^{\bullet}$ / $HO_2^{\bullet}$. The tendency of O_3 generation was thus more limited by the responses of $RO_2^{\bullet}$ / $HO_2^{\bullet}$ + NO (Martin et al., 2004). Therefore, the O_3 formation in Chinese cities became more sensitive to NO_x in recent years, and is predicted to stay in transitional regime till 2030 (Jin and Holloway, 2015). Our finding provides an effective O_3 control route to Luoyang where is being challenged by the inherent controls. The results also verified the NO_x control progress in China and supported strict NO_x control strategies in the future.

4. Conclusion

A comprehensive study on source apportionment of VOCs in Luoyang was conducted in summertime. Four pollution sources, including industrial, traffic, biogenic and residential, were apportioned, with average contributions of 38.4%, 32.0%, 15.8% and 13.8%, respectively. Good consistency of source apportionment results between online and offline monitoring demonstrated the effectiveness of the time-selective sampling scheme. The source apportionment results well explained the characteristics of ambient VOCs in Luoyang, further provided solid data basis for the VOC and O_3 control. Good consistency on source apportionment results was demonstrated with online and offline measurement methods. With the application of the WRF-CHEM model, both local emissions, meteorological factors, concentrations of pollutants, and their atmospheric reactions were taken account in the simulations. The model successfully simulated the variation of O_3 concentrations in Luoyang with IOA of 0.85 and MB of 5.4 μg m^{-3}. The sensitive tests indicated that 43.5% of the O_3 in Luoyang was derived from regional transportation, while 63.6% was from local emissions but 7.1% was lost

Table 3
Contribution of six local sources to maximum 8-h average O_3 concentration in Luoyang (ppbv).

Date	O_3 concentration	Agricultural	industry	Power plant	residential	traffic	biogenic
07.21	139.2	4.6	1.7	1.8	3.0	28.4	18.3
07.22	102.3	−4.5	−3.5	−4.1	−0.8	27.8	17.7
07.23	169.9	−0.7	−1.4	0.4	−0.4	25.1	31.7
07.24	174.2	2.6	−0.1	0.4	12.4	35.0	22.3
07.25	183.3	−0.2	2.6	7.2	6.3	44.8	32.1
07.26	177.1	12.4	7.4	20.2	5.2	55.1	45.3
07.27	151.0	10.3	−2.3	9.1	−2.5	35.7	33.7
Period Average	156.7	3.5	0.6	5.0	3.3	36.0	28.7

Table 4
Contributions of local sources to maximum 8-h average O_3 concentration in Luoyang (μg m^{-3}).

Date	O_3 concentration	Agricultural	Industrial	Power plant	Residential	Traffic	Biogenic
7/21	139.2	4.6	1.7	1.8	3.0	28.4	18.3
7/22	102.3	−4.5	−3.5	−4.1	−0.8	27.8	17.7
7/23	169.9	−0.7	−1.4	0.4	−0.4	25.1	31.7
7/24	174.2	2.6	−0.1	0.4	12.4	35.0	22.3
7/25	183.3	−0.2	2.6	7.2	6.3	44.8	32.1
7/26	177.1	12.4	7.4	20.2	5.2	55.1	45.3
7/27	151.0	10.3	−2.3	9.1	−2.5	35.7	33.7
Average	**156.7**	**3.5**	**0.6**	**5.0**	**3.3**	**36.0**	**28.7**

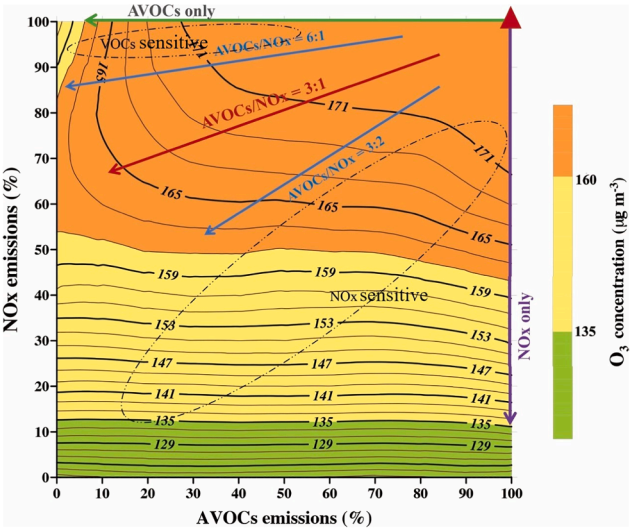

Fig. 9. The O_3 concentration isopleths in Luoyang in the afternoon (12: 00–19: 00 LT) (Triangle is the present status of atmosphere in Luoyang; the arrows were the emission reduction ratios of NOx and AVOCs; ellipses showed the typical zone of VOC-sensitive or NO_x-sensitive regime).

in the interactions. The extremely high contribution of regional transportation reveled that joint regional control policy is necessary. Traffic and biogenic were the two most prominent local sources in Luoyang, while agricultural and residential sources were negligible. The O_3 isopleths clearly indicated a transitional regime on the atmospheric formation of O_3. It also inferred that the O_3 formation would shift to NO_x regime when 45% of NO_x could be reduced in Luoyang. Disaggregating the spatial and temporal emission inventories, applying FSA module, neglecting of boundary layer vertical O_3 transportation and observing the changes in relatively short episode all feasibly contributed to the nonnegligible uncertainty of the results in this study, which would be specifically salved in the tracking study. Despite these, our results were consistent with the latest studies conducted in the megacities in China such as Beijing and Shanghai. This indicated that the stricter local and regional controls would be effective in reducing tropospheric O_3 in Luoyang.

CRediT authorship contribution statement

Jian Sun: Writing - original draft, Visualization. **Zhenxing Shen:** Conceptualization, Supervision, Resources. **Ruonan Wang:** Data curation, Investigation. **Guohui Li:** Methodology, Software. **Yue Zhang:** Formal analysis, Data curation. **Bin Zhang:** Data curation. **Kun He:** . **Zhuoyue Tang:** . **Hongmei Xu:** Data curation, Validation. **Linli Qu:** Formal analysis. **Steven Sai Hang Ho:** Writing - review & editing. **Suixin Liu:** Resources, Visualization. **Junji Cao:** Project administration.

Declaration of Competing Interest

The authors declare that they have no known competing financial interests or personal relationships that could have appeared to influence the work reported in this paper.

Acknowledgement

This research was supported by the Natural Science Foundation of China (41907188), Natural Science Foundation of Shaanxi Province, China (2019JQ-386), China Postdoctoral Science Foundation (2019M653658).

Appendix A. Supplementary material

Supplementary data to this article can be found online at https://doi.org/10.1016/j.envint.2020.106279.

References

An, J., Wang, J., Zhang, Y., Zhu, B., 2017. Source apportionment of volatile organic compounds in an urban environment at the Yangtze River Delta, China. Arch. Environ. Contam. Toxicol. 72, 335–348.
An, J., Wang, Y., Wu, F., Zhu, B., 2012. Characterizations of volatile organic compounds during high ozone episodes in Beijing, China. Environ. Monit. Assess. 184, 1879–1889.
Arghavani, S., Malakooti, H., Bidokhti, A.A., 2019. Numerical evaluation of urban green space scenarios effects on gaseous air pollutants in Tehran Metropolis based on WRF-Chem model. Atmos. Environ. 214, 116832.
Bei, N., Lei, W., Zavala, M., Molina, L.T., 2010. Ozone predictabilities due to meteorological uncertainties in the Mexico City basin using ensemble forecasts. Atmos. Chem. Phys. 10, 6295–6309.
Bei, N., Li, G., Molina, L.T., 2012. Uncertainties in SOA simulations due to meteorological uncertainties in Mexico City during MILAGRO-2006 field campaign. Atmos. Chem. Phys. 12, 11295–11308.
Binkowski, F.S., Roselle, S.J., 2003. Models-3 community multiscale air quality (CMAQ) model aerosol component 1. Model description. J. Geophysical Res.: Atmos. 108.
Bocquet, M., Elbern, H., Eskes, H., Hirtl, M., Žabkar, R., Carmichael, G.R., Flemming, J., Inness, A., Pagowski, M., Pérez Camaño, J.L., Saide, P.E., San Jose, R., Sofiev, M., Vira, J., Baklanov, A., Carnevale, C., Grell, G., Seigneur, C., 2015. Data assimilation in atmospheric chemistry models: current status and future prospects for coupled chemistry meteorology models. Atmos. Chem. Phys. 15, 5325–5358.
Carter, W.P., 2009. Carter W P L. Updated maximum incremental reactivity scale and hydrocarbon bin reactivities for regulatory applications. California Air Resources Board Contract 2009, 339.
Chen, D., Li, Q., Stutz, J., Mao, Y., Zhang, L., Pikelnaya, O., Tsai, J.Y., Haman, C., Lefer, B., Rappenglück, B., Alvarez, S.L., Neuman, J.A., Flynn, J., Roberts, J.M., Nowak, J.B., de Gouw, J., Holloway, J., Wagner, N.L., Veres, P., Brown, S.S., Ryerson, T.B., Warneke, C., Pollack, I.B., 2013. WRF-Chem simulation of NOx and O3 in the L.A. basin during CalNex-2010. Atmos. Environ. 81, 421–432.
Chen, F., Dudhia, J., 2001. Coupling an advanced land surface–hydrology model with the Penn State–NCAR MM5 modeling system. Part I: Model implementation and sensitivity. Mon. Weather Rev. 129, 569–585.
Chen, L.W.A., Cao, J., 2018. PM2.5 source apportionment using a hybrid environmental receptor model. Environ. Sci. Technol. 52, 6357–6369.
Cui, L., Zhang, Z., Huang, Y., Lee, S.C., Blake, D.R., Ho, K.F., Wang, B., Gao, Y., Wang, X. M., Louie, P.K.K., 2016. Measuring OVOCs and VOCs by PTR-MS in an urban roadside microenvironment of Hong Kong: relative humidity and temperature dependence, and field intercomparisons. Atmospheric measurement techniques.
Ding, A.J., Wang, T., Thouret, V., Cammas, J.P., Nédélec, P., 2008. Tropospheric ozone climatology over Beijing: analysis of aircraft data from the MOZAIC program. Atmos. Chem. Phys. 8, 1–13.
Dudhia, J., 1989. Numerical study of convection observed during the winter monsoon experiment using a mesoscale two-dimensional model. J. Atmos. Chem. 46, 3077–3107.

Feng, T., Bei, N., Huang, R.J., Cao, J., Zhang, Q., Zhou, W., Tie, X., Liu, S., Zhang, T., Su, X., Lei, W., Molina, L.T., Li, G., 2016. Summertime ozone formation in Xi'an and surrounding areas. China. Atmos. Chem. Phys. 16, 4323–4342.
Feng, T., Bei, N., Zhao, S., Wu, J., Li, X., Zhang, T., Cao, J., Zhou, W., Li, G., 2018. Wintertime nitrate formation during haze days in the Guanzhong basin, China: A case study. Environ. Pollut. 243, 1057–1067.
Gaudel, A., Cooper, O. R., Ancellet, G., Barret, B., Ziemke, J., 2018. Tropospheric Ozone Assessment Report: Present-day distribution and trends of tropospheric ozone relevant to climate and global atmospheric chemistry model evaluation.
Grell, G.A., Peckham, S.E., Schmitz, R., McKeen, S.A., Frost, G., Skamarock, W.C., Eder, B., 2005. Fully coupled "online" chemistry within the WRF model. Atmos. Environ. 39, 6957–6975.
Gu, Y., Li, Q., Wei, D., Gao, L., Tan, L., Su, G., Liu, G., Liu, W., Li, C., Wang, Q., 2019. Emission characteristics of 99 NMVOCs in different seasonal days and the relationship with air quality parameters in Beijing, China. Ecotoxicol. Environ. Saf. 169, 797–806.
Guenther, A., Karl, T., Harley, P., Wiedinmyer, C., Palmer, P., Geron, C., 2006. Estimates of global terrestrial isoprene emissions using MEGAN (Model of Emissions of Gases and Aerosols from Nature).
Guo, J., He, J., Liu, H., Miao, Y., Liu, H., Zhai, P., 2016. Impact of various emission control schemes on air quality using WRF-Chem during APEC China 2014. Atmos. Environ. 140, 311–319.
Ho, S.S.H., Chow, J.C., Watson, J.G., Wang, L., Qu, L., Dai, W., Huang, Y., Cao, J., 2017. Influences of relative humidities and temperatures on the collection of C-2-C-5 aliphatic hydrocarbons with multi-bed (Tenax TA, Carbograph 1TD, Carboxen 1003) sorbent tube method. Atmos. Environ. 151, 45–51.
Ho, S.S.H., Wang, L., Chow, J.C., Watson, J.G., Xue, Y., Huang, Y., Qu, L., Li, B., Dai, W., Li, L., Cao, J., 2018. Optimization and evaluation of multi-bed adsorbent tube method in collection of volatile organic compounds. Atmos. Res. 202, 187–195.
Hong, S.-Y., Lim, J.-O.J., 2006. The WRF single-moment 6-class microphysics scheme (WSM6). Asia-Pac. J. Atmos. Sci. 42, 129–151.
Hopke, P.K., 2016. Review of receptor modeling methods for source apportionment. J. Air Waste Manag. Assoc. 66, 237–259.
Huang, X., Zhang, Y., Yang, W., Huang, Z., Wang, Y., Zhang, Z., He, Q., Lü, S., Huang, Z., Bi, X., Wang, X., 2017. Effect of traffic restriction on reducing ambient volatile organic compounds (VOCs): Observation-based evaluation during a traffic restriction drill in Guangzhou, China. Atmos. Environ. 161, 61–70.
Hui, L., Liu, X., Tan, Q., Feng, M., An, J., Qu, Y., Zhang, Y., Deng, Y., Zhai, R., Wang, Z., 2020. VOC characteristics, chemical reactivity and sources in urban Wuhan, central China. Atmos. Environ. 224, 117340.
Hui, L., Liu, X., Tan, Q., Feng, M., An, J., Qu, Y., Zhang, Y., Jiang, M., 2018. Characteristics, source apportionment and contribution of VOCs to ozone formation in Wuhan, Central China. Atmos. Environ. 192, 55–71.
Janić, Z.I., 2001. Nonsingular implementation of the Mellor-Yamada level 2.5 scheme in the NCEP Meso model.
Jin, X., Holloway, T., 2015. Spatial and temporal variability of ozone sensitivity over China observed from the Ozone Monitoring Instrument. J. Geophys. Res.: Atmos. 120, 7229–7246.
Kelly, J.M., Doherty, R.M., O'Connor, F.M., Mann, G.W., 2018. The impact of biogenic, anthropogenic, and biomass burning volatile organic compound emissions on regional and seasonal variations in secondary organic aerosol. Atmos. Chem. Phys. 18, 7393–7422.
Kleindienst, T.E., Jaoui, M., Lewandowski, M., Offenberg, J.H., Lewis, C.W., Bhave, P.V., Edney, E.O., 2007. Estimates of the contributions of biogenic and anthropogenic hydrocarbons to secondary organic aerosol at a southeastern US location. Atmos. Environ. 41, 8288–8300.
Kumar, A., Singh, D., Kumar, K., Singh, B.B., Jain, V.K., 2018. Distribution of VOCs in urban and rural atmospheres of subtropical India: Temporal variation, source attribution, ratios, OFP and risk assessment. Sci. Total Environ. 613–614, 492–501.
LBS, L. b. o. s., 2018. Statistical year book of Luoyang, 2018. http://www.lytjj.gov.cn/sitesources/lystjj/page_pc/tjsj/tjnj/article84afc9205f284267abf3797fc157fbfe.html.
Le, T., Wang, Y., Liu, L., Yang, J., Yung, Y.L., Li, G., Seinfeld, J.H., 2020. Unexpected air pollution with marked emission reductions during the COVID-19 outbreak in China. Science 369, 702–706.
Lee, S.C., Chiu, M.Y., Ho, K.F., Zou, S.C., Wang, X., 2002. Volatile organic compounds (VOCs) in urban atmosphere of Hong Kong. Chemosphere 48, 375–382.
Li, G., Bei, N., Cao, J., Wu, J., Long, X., Feng, T., Dai, W., Liu, S., Zhang, Q., Tie, X., 2017a. Widespread and persistent ozone pollution in eastern China during the non-winter season of 2015: observations and source attributions. Atmos. Chem. Phys. 17.
Li, G., Bei, N., Cao, J., Wu, J., Long, X., Feng, T., Dai, W., Liu, S., Zhang, Q., Tie, X., 2017b. Widespread and persistent ozone pollution in eastern China during the non-winter season of 2015: observations and source attributions. Atmos. Chem. Phys. 17, 2759–2774.
Li, G., Bei, N., Tie, X., Molina, L., 2011. Aerosol effects on the photochemistry in Mexico City during MCMA-2006/MILAGRO campaign.
Li, G., Lei, W., Bei, N., Molina, L., 2012. Contribution of garbage burning to chloride and PM 2.5 in Mexico City.
Li, G., Lei, W., Zavala, M., Volkamer, R., Dusanter, S., Stevens, P., Molina, L., 2010. Impacts of HONO sources on the photochemistry in Mexico City during the MCMA-2006/MILAGO Campaign.
Li, N., He, Q., Greenberg, J., Guenther, A., Li, J., Cao, J., Wang, J., Liao, H., Wang, Q., Zhang, Q., 2018a. Impacts of biogenic and anthropogenic emissions on summertime ozone formation in the Guanzhong Basin, China. Atmos. Chem. Phys. 18, 7489.
Li, X.Y., Li, S.J., Liu, P.F., Kong, Y.F., Song, H.Q., 2018b. Spatial and temporal variations of ozone concentrations in China in 2016. Acta Scientiae Circumstantiae 38, 1263–1274.
Liu, Y., Shao, M., Fu, L., Lu, S., Zeng, L., Tang, D., 2008a. Source profiles of volatile organic compounds (VOCs) measured in China: Part I. Atmos. Environ. 42, 6247–6260.
Liu, Y., Shao, M., Lu, S., Chang, C.-C., Wang, J.-L., Fu, L., 2008b. Source apportionment of ambient volatile organic compounds in the Pearl River Delta, China: Part II. Atmos. Environ. 42, 6261–6274.
Liu, Y., Wang, H., Jing, S., Gao, Y., Peng, Y., Lou, S., Cheng, T., Tao, S., Li, L., Li, Y., Huang, D., Wang, Q., An, J., 2019. Characteristics and sources of volatile organic compounds (VOCs) in Shanghai during summer: Implications of regional transport. Atmos. Environ. 215, 116902.
Luecken, D.J., Napelenok, S.L., Strum, M., Scheffe, R., Phillips, S., 2018. Sensitivity of ambient atmospheric formaldehyde and ozone to precursor species and source types across the United States. Environ. Sci. Technol. 52, 4668–4675.
Lupaşcu, A., Butler, T., 2019. Source attribution of European surface O3 using a tagged O3 mechanism. Atmos. Chem. Phys. 19, 14535–14558.
Lyu, X., Wang, N., Guo, H., Xue, L., Jiang, F., Zeren, Y., Cheng, H., Cai, Z., Han, L., Zhou, Y., 2019. Causes of a continuous summertime O-3 pollution event in Jinan, a central city in the North China Plain. Atmospheric Chemistry and Physics.
Lyu, X.P., Chen, N., Guo, H., Zhang, W.H., Wang, N., Wang, Y., Liu, M., 2016. Ambient volatile organic compounds and their effect on ozone production in Wuhan, central China. Sci. Total Environ. 541, 200–209.
Martin, R.V., Fiore, A.M., Van Donkelaar, A., 2004. Space-based diagnosis of surface ozone sensitivity to anthropogenic emissions. Geophys. Res. Lett. 31.
Mo, Z., Shao, M., Wang, W., Liu, Y., Wang, M., Lu, S., 2018. Evaluation of biogenic isoprene emissions and their contribution to ozone formation by ground-based measurements in Beijing, China. Sci. Total Environ. 627, 1485–1494.
Pollack, I.B., Ryerson, T.B., Trainer, M., Parrish, D.D., Andrews, A.E., Atlas, E.L., Blake, D.R., Brown, S.S., Commane, R., Daube, B.C., de Gouw, J.A., Dubé, W.P., Flynn, J., Frost, G.J., Gilman, J.B., Grossberg, N., Holloway, J.S., Kofler, J., Kort, E. A., Kuster, W.C., Lang, P.M., Lefer, B., Lueb, R.A., Neuman, J.A., Nowak, J.B., Novelli, P.C., Peischl, J., Perring, A.E., Roberts, J.M., Santoni, G., Schwarz, J.P., Spackman, J.R., Wagner, N.L., Warneke, C., Washenfelder, R.A., Wofsy, S.C., Xiang, B., 2012. Airborne and ground-based observations of a weekend effect in ozone, precursors, and oxidation products in the California South Coast Air Basin. J. Geophys. Res.: Atmos. 117.
Ryu, Y.-H., Hodzic, A., Descombes, G., Hu, M., Barré, J., 2019. Toward a better regional ozone forecast over CONUS using rapid data assimilation of clouds and meteorology in WRF-Chem. J. Geophys. Res.: Atmos. 124, 13576–13592.
Shao, P., An, J., Xin, J., Wu, F., Wang, J., Ji, D., Wang, Y., 2016. Source apportionment of VOCs and the contribution to photochemical ozone formation during summer in the typical industrial area in the Yangtze River Delta, China. Atmos. Res. 176–177, 64–74.
Shen, Z., Cao, J., Zhang, L., Zhao, Z., Dong, J., Wang, L., Wang, Q., Li, G., Liu, S., Zhang, Q., 2014. Characteristics of surface O3 over Qinghai Lake area in Northeast Tibetan Plateau, China. Sci. Total Environ. 500–501, 295–301.
Su, X., Tie, X., Li, G., Cao, J., Huang, R., Feng, T., Long, X., Xu, R., 2017. Effect of hydrolysis of N2O5 on nitrate and ammonium formation in Beijing China: WRF-Chem model simulation. Sci. Total Environ. 579, 221–229.
Sun, J., Shen, Z., Zhang, Y., Zhang, Z., Zhang, Q., Zhang, T., Niu, X., Huang, Y., Cui, L., Xu, H., Liu, H., Cao, J., Li, X., 2019. Urban VOC profiles, possible sources, and its role in ozone formation for a summer campaign over Xi'an, China. Environ. Sci. Pollut. Res. 26, 27769–27782.
Tan, Z., Lu, K., Jiang, M., Su, R., Dong, H., Zeng, L., Xie, S., Tan, Q., Zhang, Y., 2018. Exploring ozone pollution in Chengdu, southwestern China: A case study from radical chemistry to O3-VOC-NOx sensitivity. Sci. Total Environ. 636, 775–786.
Tie, X., Madronich, S., Li, G., Ying, Z., Zhang, R., Garcia, A.R., Lee-Taylor, J., Liu, Y., 2007. Characterizations of chemical oxidants in Mexico City: A regional chemical dynamical model (WRF-Chem) study. Atmos. Environ. 41, 1989–2008.
Tsai, J.-H., Chang, S.-Y., Chiang, H.-L., 2012. Volatile organic compounds from the exhaust of light-duty diesel vehicles. Atmos. Environ. 61, 499–506.
Verstraeten, W.W., Neu, J.L., Williams, J.E., Bowman, K.W., Worden, J.R., Boersma, K.F., 2015. Rapid increases in tropospheric ozone production and export from China. Nat. Geosci. 8, 690.
Wang, J., Jin, L., Gao, J., Shi, J., Zhao, Y., Liu, S., Jin, T., Bai, Z., Wu, C.-Y., 2013. Investigation of speciated VOC in gasoline vehicular exhaust under ECE and EUDC test cycles. Sci. Total Environ. 445–446, 110–116.
Wang, L., Zhang, Y., Wang, K., Zheng, B., Zhang, Q., Wei, W., 2016. Application of weather research and forecasting model with chemistry (WRF/Chem) over northern China: Sensitivity study, comparative evaluation, and policy implications. Atmos. Environ. 124, 337–350.
Wang, N., Lyu, X., Deng, X., Huang, X., Jiang, F., Ding, A., 2019a. Aggravating O3 pollution due to NOx emission control in eastern China. Sci. Total Environ. 677, 732–744.
Wang, R., Tie, X., Li, G., Zhao, S., Long, X., Johansson, L., An, Z., 2019b. Effect of ship emissions on O3 in the Yangtze River Delta region of China: Analysis of WRF-Chem modeling. Sci. Total Environ. 683, 360–370.
Wang, R., Xu, X., Jia, S., Ma, R., Ran, L., Deng, Z., Lin, W., Wang, Y., Ma, Z., 2017a. Lower tropospheric distributions of O3 and aerosol over Raoyang, a rural site in the North China Plain. Atmos. Chem. Phys. 17, 3891–3903.
Wang, T., Xue, L., Brimblecombe, P., Lam, Y.F., Li, L., Zhang, L., 2017b. Ozone pollution in China: A review of concentrations, meteorological influences, chemical precursors, and effects. Sci. Total Environ. 575, 1582–1596.

Wei, W., Li, Y., Wang, Y., Cheng, S., Wang, L., 2018. Characteristics of VOCs during haze and non-haze days in Beijing, China: Concentration, chemical degradation and regional transport impact. Atmos. Environ. 194, 134–145.
Wesely, M.L., 2007. Parameterization of surface resistances to gaseous dry deposition in regional-scale numerical models. Atmos. Environ. 41, 52–63.
Wu, J., Bei, N., Hu, B., Liu, S., Wang, Y., Shen, Z., Li, X., Liu, L., Wang, R., Liu, Z., Cao, J., Tie, X., Molina, L.T., Li, G., 2020. Aerosol–photolysis interaction reduces particulate matter during wintertime haze events. Proc. Natl. Acad. Sci. 117, 9755–9761.
Wu, J., Bei, N., Li, X., Cao, J., Feng, T., Wang, Y., Tie, X., Li, G., 2018a. Widespread air pollutants of the North China Plain during the Asian summer monsoon season: a case study. Atmos. Chem. Phys. 18, 8491–8504.
Wu, J., Bei, N., Li, X., Cao, J., Feng, T., Wang, Y., Tie, X., Li, G., 2018b. Widespread air pollutants of the North China Plain during the Asian summer monsoon season: A case study. Atmos. Chem. Phys. 1–36.
Wu, X., Wu, Y., Zhang, S., Liu, H., Fu, L., Hao, J., 2016. Assessment of vehicle emission programs in China during 1998–2013: Achievement, challenges and implications. Environ. Pollut. 214, 556–567.
Xing, J., Wang, S.X., Jang, C., Zhu, Y., Hao, J.M., 2011. Nonlinear response of ozone to precursor emission changes in China: a modeling study using response surface methodology. Atmos. Chem. Phys. 11, 5027–5044.
Yamada, H., 2013. Contribution of evaporative emissions from gasoline vehicles toward total VOC emissions in Japan. Sci. Total Environ. 449, 143–149.
Ye, L., Wang, X., Fan, S., Chen, W., Chang, M., Zhou, S., Wu, Z., Fan, Q., 2016. Photochemical indicators of ozone sensitivity: application in the Pearl River Delta, China. Frontiers Environ. Sci. Eng. 10, 15.
Zhang, L., Li, Q.Y., Wang, T., Ahmadov, R., Zhang, Q., Li, M., Lv, M.Y., 2017. Combined impacts of nitrous acid and nitryl chloride on lower-tropospheric ozone: new module development in WRF-Chem and application to China. Atmos. Chem. Phys. 17(16), 9733–9750, 17.
Zhang, Q., Streets, D.G., Carmichael, G.R., He, K., Huo, H., Kannari, A., Klimont, Z., Park, I., Reddy, S., Fu, J., 2009. Asian emissions in 2006 for the NASA INTEX-B mission. Atmos. Chem. Phys. 9, 5131–5153.
Zhang, Z., Zhang, Y., Wang, X., Lü, S., Huang, Z., Huang, X., Yang, W., Wang, Y., Zhang, Q., 2016. Spatiotemporal patterns and source implications of aromatic hydrocarbons at six rural sites across China's developed coastal regions. J. Geophys. Res.: Atmos. 121, 6669–6687.